ACS SENSORS

pubs.acs.org/acssensors

Article

Pure Covalent-Organic Framework Membrane as a Label-Free Biomimetic Nanochannel for Sensitive and Selective Sensing of Chiral Flavor Substances

Chen-Yan Zheng, Hai-Long Qian, Cheng Yang, Xu-Qin Ran, and Xiu-Ping Yan*

Cite This: *ACS Sens.* 2023, 8, 4747−4755

Read Online

ACCESS | Metrics & More | Article Recommendations | Supporting Information

ABSTRACT: Chiral flavor substances play an important role in the human perception of different tastes. Here, we report a pure covalent-organic framework (COF) membrane nanochannel in combination with a chiral gold nanoparticles (AuNPs) selector for sensing chiral flavor substances. The pure COF membrane with a proper pore size is selected as the nanochannel, while L-cysteine-modified AuNPs (L-Cys-AuNPs) are used as the chiral selector. L-Cys-AuNPs show stronger binding to the *S*-enantiomer than the *R*-enantiomer, causing current reduction to different degrees for the *R*- and *S*-enantiomer to achieve chiral sensing due to the synergistic effect of the size exclusion of the COF nanochannel and the chiral selectivity of L-Cys-AuNPs. The developed COF membrane nanochannel sensing platform not only allows an easy balance of the permeability and selectivity, which is difficult to achieve in traditional polymer membrane nanochannel sensors, but also exhibits better chiral performance than commercial artificial anodic aluminum oxide (AAO) nanochannel sensors. The developed nanochannel sensor is successfully applied for sensing flavor enantiomers such as limonene, propanediol, methylbutyric acid, and butanol with the enantiomer excess values of 55.2% (propanediol) and 72.4% (limonene) and the low detection limits of 36 (limonene) and 71 (propanediol) ng L^{-1}. This study provides a new idea for the construction of nanochannel platforms based on the COF for sensitive and selective chiral sensing.

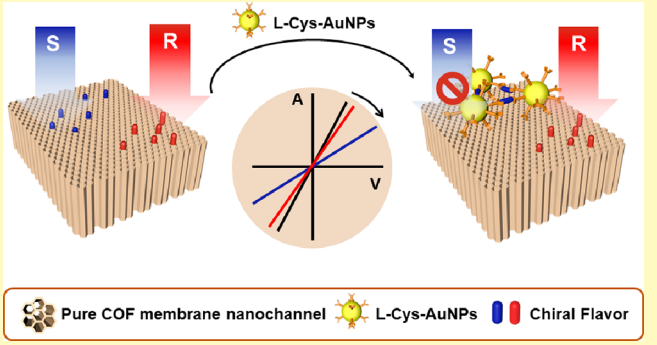

KEYWORDS: *covalent-organic frameworks, nanochannels, chiral gold nanoparticles, chiral sensing, chiral flavor substances*

Chirality means a pair of molecules that mirror each other in stereochemistry and whose spatial structures cannot overlap.[1−3] Enantiomers have identical physical properties but significant differences in chiral environments such as biomedicine and environmental effects. For example, *S*-naproxen has a higher pharmacological activity than *R*-naproxen, while only the *R*-isomer of phenoxy alkanoic acid has herbicidal activity. Interestingly, chiral flavor substances also play an important role in the process of the human perception of different tastes. Different enantiomers of chiral flavor substances may interact in different ways with receptors, transport systems, or enzymes, resulting in different flavors or aromas in humans, such as *R*- and *S*-limonene with orange flavor and lemon flavor, respectively,[4] and *R*- and *S*-3-mercapto-1-hexanol with grapefruit aroma and passion fruit aroma, respectively.[5] The sensing of chiral flavor substances helps to distinguish key aroma components and understand the human need for manual flavor substances.[6−9] Moreover, evaluating chiral flavor substances in food is essential not only to improve food quality but also to guide public healthy eating behavior.

Up to now, a variety of techniques for the chiral identification of flavor substances have been reported, such as chromatography,[10,11] spectroscopy,[12,13] and electronic tongues.[14−16] Although these methods have their own advantages in specificity, accuracy, and sensitivity, they still have a variety of drawbacks, such as cumbersome operation and limited performance, which cannot meet the growing needs of advanced bioanalysis.[17−20] Therefore, it is urgent to develop a sensitive and selective sensing method to ensure the safety of related chiral flavor substances.

Nanochannel sensing technology has attracted much attention because of its advantages of high sensitivity, fast response, and easy miniaturization.[21−26] It effectively integrates the Coulter counting method and channel ion current

Received: September 3, 2023
Revised: October 20, 2023
Accepted: November 16, 2023
Published: December 6, 2023

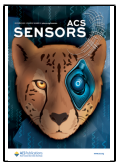

measurement and generally refers to planar or tubular structures with pore sizes in the range of 1−100 nm.[27,28] Since the scale of the pore size of nanochannels drops to nanometers, various surface forces (such as steric hindrance, van der Waals forces, and electrostatic forces) induce unique behaviors different from macroscopic transmission when molecules or ions pass through the pores.[29−33] Nanochannels usually exhibit three characteristics: ion gating, ion selectivity, and ion rectification. A variety of chiral sensors based on the transport mechanisms of drugs/metabolites transporter (DMT) and transmembrane proteins in nature have been reported.[34−38] Yan et al. have carried out theoretical calculations to further understand the ion transfer effect of the nanochannel.[39] Han et al. incorporated a chiral identification unit (β-cyclodextrin) into the polyethylene terephthalate (PET) channel to design a cone-shaped nanochannel chiral recognition sensor for the highly selective identification of histidine enantiomers.[40] Sun et al. used bovine serum albumin as a chiral selector for a label-free PET nanochannel to identify arginine enantiomers.[41] Meng et al. prepared a chiral nanochannel membrane (penicillamine-modified $Cu_{2-x}Se$/AAO (anodic aluminum oxide)) with high ionic rectification characteristics and strong chirality for sensitive identification of naproxen enantiomers.[42] Most nanochannel membranes rely on the monolayer of chiral receptors on the traditional polymer membrane surface to achieve chiral recognition. However, it is difficult for traditional polymer membrane nanochannels to balance the permeability and selectivity. Therefore, exploring novel nanochannel materials and chiral recognition mechanisms is one of the main challenges in constructing chiral nanochannel sensors.

Covalent-organic frameworks (COFs) have shown promising applications in the emerging field of nanochannel analysis. COFs, a class of organic porous crystalline materials consisting of light elements (C, O, N, B, etc.) linked by covalent bonds, have attracted much attention because of their large porosity, well-defined pore structure, and controllable pore size.[43−46] Yuan et al. reported a chiral sensor based on β-cyclodextrin-modified COF mixed matrix membrane for the separation of histidine enantiomers.[47] Ran et al. prepared AAO nanochannel sensors based on thiourea-linked 2D COFs for the rapid and sensitive detection of Hg(II) in real samples.[48] Pure COF membrane nanochannels can make full use of the advantages of COFs[49,50] but difficult to postmodify due to their weak mechanical strength. So far, no works have been reported on a pure COF membrane nanochannel platform for chiral sensing.

Herein, we report a label-free biomimetic pure COF membrane nanochannel platform in conjunction with a chiral gold nanoparticles (AuNPs) selector for sensing chiral flavor substances. L-Cysteine-modified AuNPs (L-Cys-AuNPs) are selected as the chiral selector to interact with the analytes, while KCl aqueous solution is used as the electrolyte. The flexible COF membrane with a pore size of 1.7 nm, synthesized from 4,4′4″-triaminotriphenylamine (TAPA) and 2,4,6-triformylphloroglucinol (TP) via interfacial polymerization,[51,52] is selected as the nanochannel platform, so that its pore size is slightly larger than the molecular size of the analytes but smaller than the molecular size of L-Cys-AuNPs and their adducts with analytes. Thus, the analytes can pass the nanochannel freely, while L-Cys-AuNPs and their adducts with analytes are excluded. The chiral selectivity of L-Cys-AuNPs makes it bind with *R*- and *S*-flavor enantiomers to a different extent, causing different degrees of current value reduction for chiral sensing. The pure COF membrane nanochannel platform gives a higher chiral selectivity than the commercial artificial AAO nanochannel (<10 nm) due to the synergistic effect of the size exclusion of the COF nanochannel and the chiral selectivity of L-Cys-AuNPs. This work provides a new way for the construction of the COF nanochannel platform for selective and sensitive chiral sensing.

EXPERIMENTAL SECTION

Materials and Chemicals. 4,4′4″-Triaminotriphenylamine (TAPA) and 2,4,6-triformylphloroglucinol (TP) were obtained from Jilin Chinese Academy of Sciences-Yanshen Technology Co. (Changchun, China). Dichloromethane (DCM), *N*,*N*-dimethylformamide (DMF), tetrahydrofuran (THF), hydrochloric acid (HCl), and ethanol (EtOH) were provided by Sinopharm Chemical Reagent Co. (Shanghai, China). Chloroauric acid ($HAuCl_4$), L-cysteine (L-Cys), D-cysteine (D-Cys), L-penicillamine (L-Pen), and D-penicillamine (D-Pen) were supplied by Macklin Biochemical Co. (Shanghai, China). (*S*)-(−)-Limonene, (*R*)-(+)-limonene, (*S*)-(+)-1,2-propanediol, (*R*)-(−)-1,2-propanediol, (*S*)-2-methylbutyric acid, (*R*)-2-methylbutyric acid, (*S*)-(+)-2-butanol, and (*R*)-(−)-2-butanol were obtained from Aladdin Chemistry Co. (Shanghai, China). Ultrapure water was purchased from Wahaha Group Co. (Hangzhou, China).

Fabrication of the Pure COF Membrane Nanochannel. The pure COF membrane nanochannel was prepared via interfacial polymerization according to a previous report.[51] First, TP (6.305 mg, 0.6 mmol) and TAPA (8.715 mg, 0.6 mmol) were dissolved in DCM (5 mL). After ultrasonication for 15 min, the mixture was poured into a glass Petri dish as the organic phase. Then, ultrapure water was added dropwise on the surface of the organic phase until a stable interface between the organic and inorganic phases was formed. Subsequently, acetic acid (60 μL, 3.0 M) was added dropwise to the inorganic phase as the catalyst. The Petri dish was sealed with a cling film to avoid gas flow. The interfacial polymerization reaction was carried out at room temperature for 48 h to form a self-standing and flexible membrane at the interface between the organic and inorganic phases. The formed membrane was washed with ultrapure water and acetone to remove the unreacted monomers, and the pure COF membrane nanochannel was thus obtained for further experiments.

Synthesis of L-Cysteine-Modified AuNPs (L-Cys-AuNPs). L-Cys-AuNPs were fabricated via a classical reaction, as described in a previous study.[57] First, $HAuCl_4$ (0.089 mg mL^{-1}) and L-cysteine (2 mM) were dissolved in ultrapure water (20 mL). Subsequently, freshly prepared $NaBH_4$ (200 μL, 0.1 M) was added dropwise to the mixture, and the mixture was stirred vigorously for 2 h. During the reaction, the color of the solution changed from light yellow to pink as the gold ions were reduced to gold atoms, indicating the successful preparation of L-Cys-AuNPs. The procedure for the synthesis of D-Cys-, L-Pen-, and D-Pen-modified AuNPs was similar to the method for preparing L-Cys-AuNPs.

Instrumentation. Scanning electron microscopy (SEM) images were collected on an S-3500N microscope (Hitachi, Japan). Powder X-ray diffraction (PXRD) data were recorded on a D2 PHASER X-ray diffractometer (Bruker, Germany) using Cu K_α radiation (λ, 1.5418 Å; step size, 0.5°; scanning speed, 8° min^{-1}). The nitrogen adsorption and desorption isotherms were measured on an Autosorb-iQ analyzer (Quantachrome, USA) at 77 K. Transmission electron microscopy (TEM) images of chiral AuNPs were observed on a Hitachi H-7650-type TEM (Hitachi, Japan). Circular dichroism (CD) spectra of the chiral AuNPs were recorded on a Chirascan V100 spectrometer (Applied Photophysics, UK). The sizes of chiral AuNPs and their adducts with analytes were measured on a Zetasizer Nano ZS system (Malvern, UK). Contact angles (CAs) were recorded on an OCA15EC video optical contact angle system (DataPhysics, Germany). All ion current measurements were performed on a homemade nanochannel analysis platform for chiral sensing.[60]

Ion Current Measurement. The homemade nanochannel analysis platform consists of a flow system including two polytetrafluoroethylene flow cells, a 2450 SourceMeter (Keithley,

https://doi.org/10.1021/acssensors.3c01849
ACS Sens. 2023, 8, 4747−4755

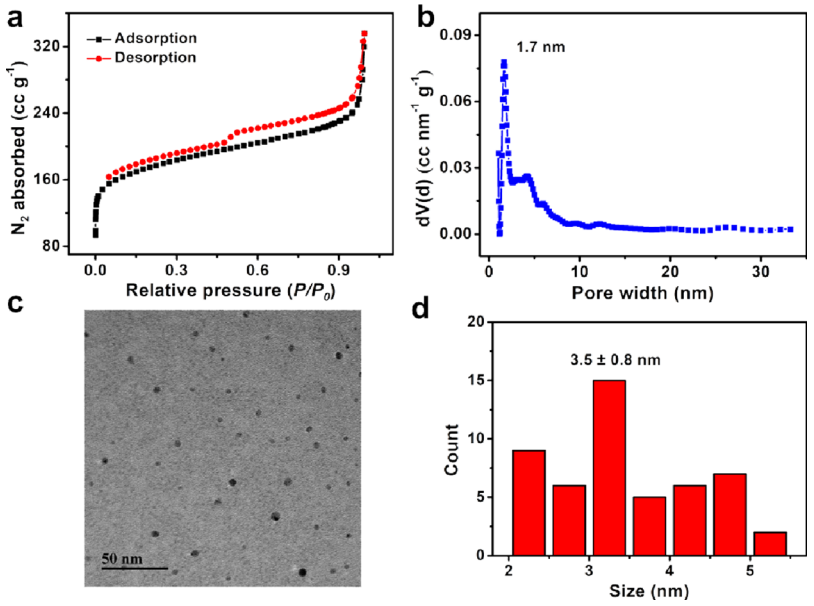

Figure 1. N_2 adsorption−desorption isotherms (a) and pore size distribution (b) of the COF membrane. TEM image (c) and histogram of particle size distribution (d) of D/L-Cys-AuNPs.

USA) and a data acquisition system (version 2.06, Keithley, USA).[60] The prepared pure COF membrane (~40 mm^2) was installed between the two poly(tetrafluoroethylene) flow cells. The Ag/AgCl electrode was inserted into each cell to measure the transmembrane ion current (transmembrane potential, −0.2 to 0.2 V; scanning rate, 0.02 V s^{-1}). The effective ion-conducting area of the COF membrane was 2.5 mm^2. The COF membrane could be repeatedly installed 6−7 times in a homemade platform. KCl was used as the electrolyte for all tests, and three parallel measurements were performed for each group of tests.

Molecular Docking Analysis. AutoDock Vina 1.2.2 was employed to analyze the binding affinities between the chiral AuNPs and chiral flavor substances. The molecular structures of chiral AuNPs and chiral flavor substances were retrieved from PubChem Compound (https://pubchem.ncbi.nlm.nih.gov/).

Finite-Element Simulation by COMSOL Multiphysics. Steady-state finite-element simulation was performed using COMSOL Multiphysics 6.0 to provide a quantitative model of the diffusion of limonene enantiomers.[53] The modules of electrostatics (es), transport of diluted species (chds), and laminar flow (spf) were used for the simulation. The diffusion coefficient of *S*/*R*-limonene was converted to the experimentally measured transport rate. The size of the pure COF membrane nanochannel was 85 × 641 nm (Φ × *L*), and one axis section contained 50 COF channels.

RESULTS AND DISCUSSION

Design, Fabrication, and Characterization of the Pure COF Membrane Nanochannel. As for the interfacial polymerization method, one of the prerequisites for the synthesis of COF membranes is that the amine monomer and aldehyde monomer can be dissolved in the inorganic phase and organic phase, respectively. Meanwhile, smaller and higher electrophilic aldehyde monomers can facilitate the reaction-diffusion process and finally achieve the facile preparation of pure COF membranes. In addition, the *β*-ketoenamine-linked COF has high stability and affinity. In addition, the pore size of the COF membrane nanochannel should be larger than the molecular size of the analytes but smaller than the molecular size of L-Cys-AuNPs and their adducts with analytes, so that the analytes can pass the nanochannel freely while L-Cys-AuNPs and their adducts with analytes are excluded. For the above reasons, TP and TAPA were selected to synthesize a self-standing COF.

Figure S1a shows the procedure for manufacturing the COF membrane. The flexible COF membrane could naturally stretch in water for nanochannel sensing (Figure S1b). The dried membrane was still flexible and smooth (Figure S2). Figure S3 shows the cross-sectional SEM images and *I*−*V* curves of the COF membrane at different synthesis times. The pure COF membrane reached a stable thickness of 641 nm after 48 h due to the unique self-sealing and self-termination properties of the interfacial polymerization. Meanwhile, the current values of COF films with different thicknesses were similar at 0.2 V (531 nm, 27.34 nA; 641 nm, 27.33 nA; 646 nm, 27.38 nA). Therefore, the 641 nm thick COF membrane was chosen to give sufficient mechanical strength and stable current for nanofluidic applications (Figure S1c). PXRD and Fourier transform infrared (FT-IR) spectroscopy were employed to study the structural characteristics of the prepared COF membrane. The COF membrane showed a diffraction peak at $2\theta = 6.27°$, which was consistent with the simulated peak for the AA stack model, indicating that the COF membrane with a one-dimensional nanochannel was successfully prepared (Figure S4a). Since TAPA and TFP underwent ketone-enol tautomeric reactions, the aldehyde characteristic peaks of TFP (~1643 and ~2898 cm^{-1}) and the amino characteristic peaks of TAPA (~3404 and ~3337 cm^{-1}) disappeared, while the FT-IR spectra of the COF membrane showed characteristic peaks at ~1582 cm^{-1} (C=C) and ~1266 cm^{-1} (C−N), suggesting the successful preparation of the *β*-ketoenamine-linked framework structures (Figure S4b).

The pore size of the COF is one of the key factors in the construction of a chiral nanochannel sensing platform. The ultrasmall nanochannel can greatly improve the selectivity for sensing.[53] The pore width of the COF membrane was calculated to be ~1.7 nm from the N_2 adsorption isotherms at 77 K (Figure 1a,b), which was larger than the molecular size of the chiral flavor substances (Figure S5). Quantum-confined superfluidics would occur in the nanochannel with pore sizes less than 10 nm.[54]

https://doi.org/10.1021/acssensors.3c01849
ACS Sens. 2023, 8, 4747−4755

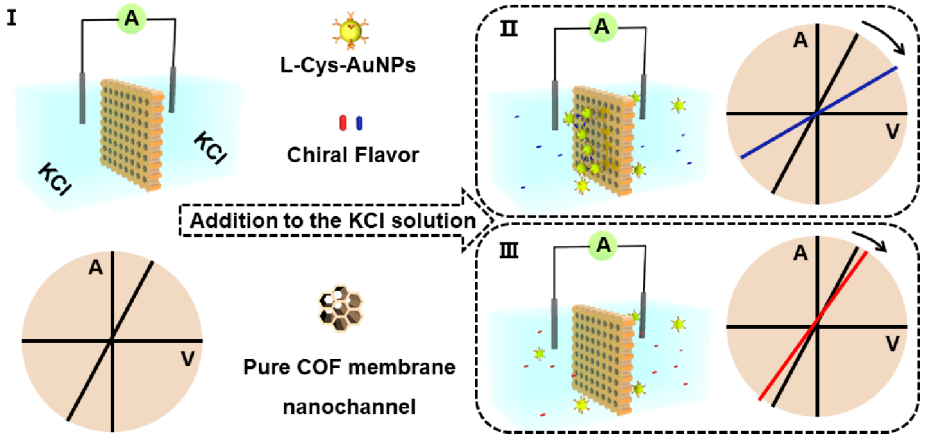

Figure 2. Schematic illustration of the developed biomimetic pure COF membrane nanochannel assay for sensing chiral flavor substances.

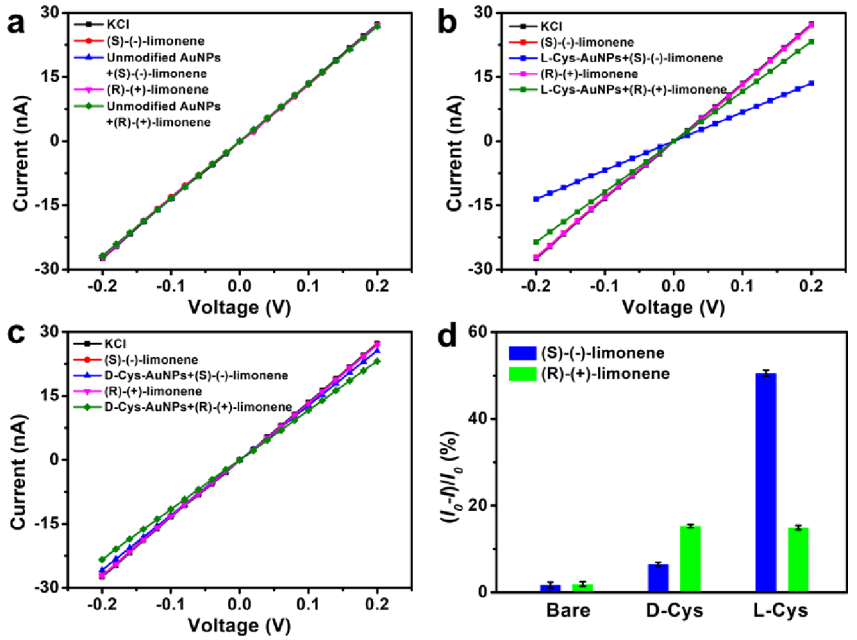

Figure 3. $I-V$ curves in KCl solution (1 μM, pH 7.14): (a) before and after adding unmodified AuNPs solution (2 mL, 1 mM) into limonene enantiomer solution (1 mg L^{-1}); (b) before and after adding L-Cys-AuNPs (2 mL, 1 mM) into limonene enantiomer solution (1 mg L^{-1}); (c) before and after adding D-Cys-AuNPs (2 mL, 1 mM) into limonene enantiomer solution (1 mg L^{-1}). (d) Comparison of the current change rates for panels (a–c). I_0 and I denote the ion current at 0.2 V without and with the addition of unmodified AuNPs and chiral AuNPs, respectively.

It is worth noting that within a certain pore size range, the larger the nanochannel, the higher is the permeance and is also conducive to the flow of analytes in the nanochannel. Thus, the chiral flavor substances can pass through the pure COF membrane nanochannel freely.

The prepared D/L-Cys-AuNPs were monodisperse nanoparticles with a size of 3.5 ± 0.8 nm (Figure 1c,d) and had a significant CD signal (Figure S6a). The particle size of D/L-Cys-AuNPs was larger than the pore size of the COF membrane (~1.7 nm) and could not pass through the nanochannel. No significant change in the hydrodynamic size (Figure S6b) and UV–vis spectra (Figure S6c) of D/L-Cys-AuNPs in 1 μM KCl solution and ultrapure water was observed within 24 h, indicating the good stability of D/L-Cys-AuNPs. In addition, the effect of D/L-Cys-AuNPs on the current value was negligible (Figure S6d), indicating that D/L-Cys-AuNPs cannot disturb the channel surface in a large area, providing a possibility for the subsequent construction of an efficient chiral nanochannel sensor.

The operation principle of the developed chiral nanochannel sensing platform is illustrated in Figure 2. The sensing of chiral flavor substances was realized by measuring the ion current flowing through the pure COF membrane nanochannel in a KCl electrolyte solution containing D/L-Cys-AuNPs. The pure COF membrane works as the ion transport nanochannel for K^+, while D/L-Cys-AuNPs serve as the chiral selector. The chiral selective binding of D/L-Cys-AuNPs to flavor enantiomers on the outer wall of the pure COF membrane disturbs the nanochannel surface, reducing the ion current to a different degree for R/S-flavor enantiomers for chiral sensing.

Ionic Transport Properties of the Fabricated Pure COF Membrane Nanochannel. The surface-charge-governed ion transport characteristics and the stability of the fabricated pure COF membrane were investigated to achieve highly sensitive chiral sensing. A pair of Ag/AgCl electrodes

https://doi.org/10.1021/acssensors.3c01849
ACS Sens. 2023, 8, 4747–4755

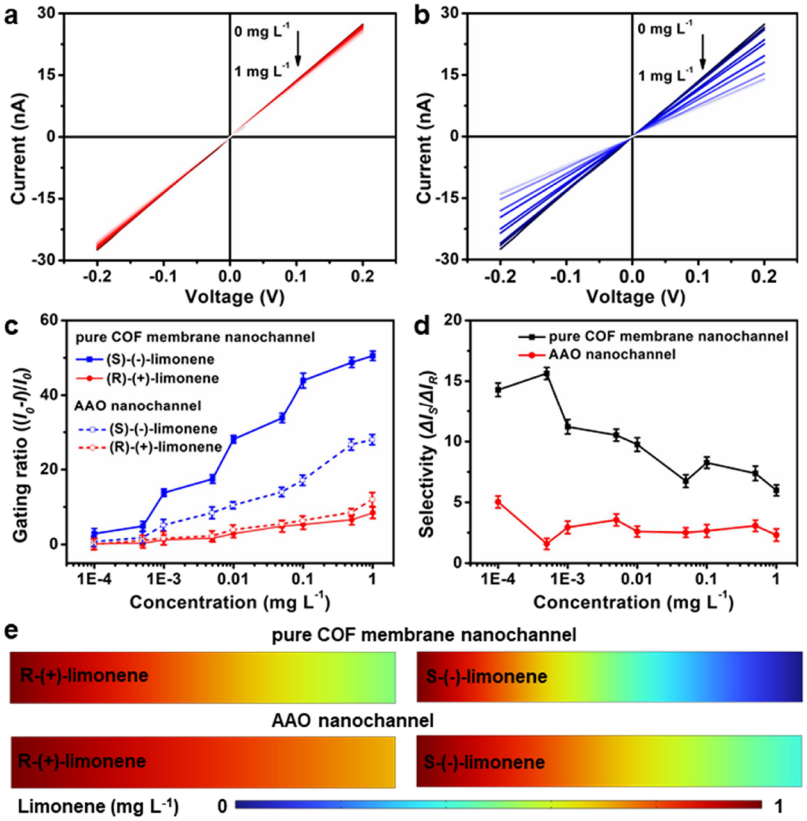

Figure 4. *I*−*V* curves of limonene enantiomers at different concentrations in the pure COF membrane nanochannel: (a) (*R*)-(+)-limonene and (b) (*S*)-(−)-limonene. Gating ratio (c) and selectivity (d) of the pure COF membrane nanochannel compared to the AAO nanochannel. (e) Simulated concentration distribution of *S*/*R*-limonene in the pure COF membrane nanochannel and AAO nanochannel.

was immersed in a homemade Teflon electrolytic cell to measure the ion current. Prior to the test, the COF membrane was soaked in a solution of KCl at various concentrations for 12 h to obtain a steady-state current. Then, the test was repeated three times for each COF membrane. Figure S7a,b shows the current−voltage (*I*−*V*) curves of the COF membrane in the solutions of KCl from 1 μM to 1 M. Because of the ultrashort ion transport path and the high porosity of the COF nanochannel, the ion current generated by the nanofluidic device based on the COF membrane (Figure S7a,b) was several orders of magnitude higher than that of the conventional AAO nanofluidic system (Figure S8).

It is worth noting that one of the important bases of chiral recognition is surface-charge-governed ion transport.[55] When the KCl electrolyte concentration was less than 0.01 M, the ionic transmembrane conductance of the COF membrane significantly deviates from the volume value (the ionic conductance of the bulk KCl electrolyte) (Figure S7c, black dashed line), indicating that the prepared COF membrane had the characteristic of the surface-charge-governed ion transport with the concentration of KCl no less than 0.01 M (Figure S7c). Meanwhile, the nanochannel size of the prepared COF membrane was much smaller than the Debye length in 1 μM KCl, suggesting that the prepared pure COF membrane nanochannel was fully negatively charged and had the characteristic of the surface-charge-governed ion transport.[56] Thus, 1 μM KCl was selected as the electrolyte in subsequent experiments.

The stability of the pure COF membrane nanochannel is also critical for sensing because of the complex environment of real sample detection. The *I*−*V* curves of the COF membrane had no significant change within 10 days (ΔI_{max} = 0.57 nA) in the KCl electrolyte (Figure S9). The symmetric transmembrane ion currents indicated that the prepared COF membrane had an insignificant asymmetric structure and high ion mobility in KCl solution.[49] Moreover, the conductance of the pure COF membrane nanochannel hardly changed in acids, alkalis, and organic solvents over 24 h (Figure S7d), indicating the good stability of the pure COF membrane nanochannel.

Chiral Sensing. AuNPs have attracted much attention due to their unique properties of inducing dynamic aggregation of analytes.[57] In our design, chiral AuNPs are selected as the chiral selectors to convert the weak chiral interaction with analytes into nanoscale aggregation behavior to obstruct ion transport in the pure COF membrane nanochannel for distinguishing chiral substances.

We took limonene enantiomers as an example to demonstrate the feasibility of the proposed chiral nanochannel sensor. To this end, the current change rate $(I_0 - I)/I_0$ after the interaction of limonene enantiomers with unmodified AuNPs, D-Cys-AuNPs, and L-Cys-AuNPs was compared (Figure 3). While the COF membrane was exposed to *R*/*S*-limonene, the ionic current hardly changed at a voltage value of 0.2 V. After injection of D/L-Cys-AuNPs into KCl solution, the electrostatic and hydrogen-bond interactions between *R*/*S*-limonene and AuNPs in KCl solution impeded ion transport within the nanochannels, reducing the ion current to a various degree for unmodified AuNPs, D-Cys-AuNPs, and L-Cys-AuNPs, respectively. The current change rate of the COF

https://doi.org/10.1021/acssensors.3c01849
ACS Sens. 2023, 8, 4747−4755

membrane nanochannel increased in the following order: unmodified AuNPs+(*S*)-(−)-limonene (1.68) < unmodified AuNPs+(*R*)-(+)-limonene (1.90) < D-Cys-AuNPs+(*S*)-(−)-limonene (6.49) < D-Cys-AuNPs+(*R*)-(+)-limonene (14.94) < L-Cys-AuNPs+(*R*)-(+)-limonene (15.30) < L-Cys-AuNPs+(*S*)-(−)-limonene (50.40). The main reason for the difference in discrimination is the different binding energies between different ligands and enantiomers (Table S1). Based on these results, L-Cys-AuNPs were selected as the chiral selector for (*S*)-(−)-limonene.

The role of the chiral ligand L-Cys is not only to stabilize AuNPs but also to recognize (*S*)-(−)-limonene.[58,59] Figure 4a,b shows the transmembrane ion currents of different concentrations of limonene enantiomers on the L-Cys-AuNPs-based pure COF membrane nanochannel sensing platform. The transmembrane ion current at 0.2 V decreased significantly with the increase of (*S*)-(−)-limonene concentration but remained almost unchanged regardless of (*R*)-(+)-limonene concentration, indicating that the prepared L-Cys-AuNPs-based pure COF membrane nanochannel enables distinguishing limonene enantiomers. Furthermore, a good linear relationship between the $(I_0 - I)/I_0$ values and the logarithms of the (*S*)-(−)-limonene concentrations was obtained in the range of 100 ng L^{-1} to 1 mg L^{-1} (Figure S10). The linear regression equation was $(I_0 - I)/I_0 = 0.1317 \lg(C_{(S)\text{-}(-)\text{-limonene}}) + 0.523$, with a determination coefficient of 0.9704 and a detection limit of 36 ng L^{-1} ($S/N = 3$). Meanwhile, the intra- and interassay precisions are listed in Table S2. Both of the RSD values were less than 5%, indicating good reproducibility of the developed nanochannel sensor. To date, no works on the pure COF membrane nanochannel platform for sensing limonene enantiomers have been reported. Compared with other limonene monitoring methods, the developed nanochannel sensor exhibited a wider linear range and a lower LOD (Table S3).

The affinity of L-Cys-AuNPs for limonene enantiomers was studied by monitoring the dynamic CA. For this purpose, limonene enantiomers (1 mg L^{-1}) were dissolved in KCl solution (1 μM) containing L-Cys-AuNPs (1 mM) to observe the CA change of the droplet on the pure COF membrane nanochannel within 2 min. At the beginning, the contact angle of the (*R*)-(+)-limonene droplet (65.4 ± 1.0°) on the pure COF membrane nanochannel was close to that of the (*S*)-(−)-limonene droplet (69.3 ± 1.0°) (Figure S11a). Then, the CAs of both *R*- and *S*-limonene droplets decreased obviously with time (Figure S11b). After 2 min, the CA of the (*R*)-(+)-limonene droplet (27.7 ± 1.0°) became significantly smaller than that of the (*S*)-(−)-limonene droplet (42.2 ± 1.0°) (Figure S11a,b), indicating that L-Cys-AuNPs had stronger binding to (*S*)-(−)-limonene than (*R*)-(+)-limonene.[53] The zeta potential of L-Cys-AuNPs (1 mM) in KCl (1 μM) containing different concentrations of limonene enantiomers was studied to further demonstrate the different aggregation behaviors of L-Cys-AuNPs relative to limonene enantiomers. L-Cys-AuNPs gave a zeta potential of −11.3 mV due to the carboxyl groups on the surface of L-Cys-AuNPs. The addition of the same concentration of limonene enantiomers to the L-Cys-AuNPs solution reduced the zeta potential due to the formation of the L-Cys-AuNPs-limonene enantiomers adducts (Figure S11c). The zeta potential change of L-Cys-AuNPs with (*S*)-(−)-limonene (from −11.3 to −0.86 mV) was still greater than that of (*R*)-(+)-limonene (from −11.3 to −3.9 mV), even if the concentration of the (*R*)-(+)-limonene enantiomer was higher by an order of magnitude, confirming that L-Cys-AuNPs had stronger affinity to (*S*)-(−)-limonene than (*R*)-(+)-limonene. Moreover, molecular docking analysis was performed to evaluate the affinity of the L-Cys to limonene enantiomers (Table S1). The results showed that L-Cys had a greater affinity for (*S*)-(−)-limonene (−0.58 kcal/mol) than for (*R*)-(+)-limonene (−0.02 kcal/mol), which was consistent with the above experimental results.

A previous study showed that the preferential interaction between L-Cys-AuNPs and enantiomers could reduce the surface charge of L-Cys-AuNPs and resulted in nanoparticle aggregation.[57] In our work, the nanoparticle size was measured by dynamic light scattering to reveal such aggregation behavior. Figure S11d shows the dependence of the aggregate size of L-Cys-AuNPs on limonene enantiomers and their concentration. The aggregates of L-Cys-AuNPs in (*S*)-(−)-limonene solution were greater than those in (*R*)-(+)-limonene solution at the same limonene concentration (>0.1 ng L^{-1}) due to the stronger affinity of L-Cys-AuNPs to (*S*)-(−)-limonene than (*R*)-(+)-limonene (Table S1). In addition, D/L-Pen-modified AuNPs also have recognition ability for limonene enantiomers (Table S4), suggesting that the preferential interaction between chiral ligands and enantiomers can induce the aggregation behavior of nanoparticles in the pure COF membrane nanochannel, thereby disturbing the transmembrane ion transport behavior.

The TEM measurement was used to further investigate L-Cys-AuNPs after exposure to limonene enantiomer solution. L-Cys-AuNPs were well dispersed in (*R*)-(+)-limonene/L-Cys-AuNPs solution but greatly aggregated in (*S*)-(−)-limonene/L-Cys-AuNPs solution (Figure S12). The results suggest the stronger interaction between (*S*)-(−)-limonene and L-Cys-AuNPs. The SEM images also show that (*S*)-(−)-limonene/L-Cys-AuNPs complexes were significantly aggregated on the surface of the COF membrane (Figure S13). The surface of the COF membrane in the absence of L-Cys-AuNPs and *R*/*S*-limonene was flat (Figure S13a). However, the surface of the COF membrane in the presence of L-Cys-AuNPs and (*S*)-(−)-limonene (Figure S13c) was rougher than that in the presence of L-Cys-AuNPs and (*R*)-(+)-limonene (Figure S13b), indicating that L-Cys-AuNPs had stronger affinity to (*S*)-(−)-limonene than (*R*)-(+)-limonene.

The selectivity of the prepared COF membrane nanochannel was compared with that of a commercial artificial AAO nanochannel to evaluate the performance of the developed COF membrane nanochannel for chiral sensing. The gating ratio of the nanochannel was defined as the current change rate $(I_0 - I)/I_0$ for enantiomers, while the selectivity ratio of the nanochannel was defined the ratio of the gating ratios and calculated as $\Delta I_S/\Delta I_R$ for limonene enantiomers. The gating ratio of the COF membrane nanochannel for (*S*)-(−)-limonene (from 2.9 to 50.5) was significantly higher than that of the AAO nanochannel (from 0.9 to 28.1) (Figure 4c). Meanwhile, the gating ratio of the pure COF membrane nanochannel to (*R*)-(+)-limonene was still very low even at high limonene concentrations. Interestingly, the chiral selectivity of the pure COF membrane nanochannel was consistently higher than that of the AAO nanochannel (Figure 4d). Moreover, the concentration distribution of limonene enantiomers in the pure COF membrane nanochannel and AAO nanochannel was simulated by COMSOL Multiphysics 6.0. Compared with the AAO nanochannel, the pure COF membrane nanochannel gave a larger concentration gradient of

https://doi.org/10.1021/acssensors.3c01849
ACS Sens. 2023, 8, 4747−4755

S-(−)-limonene (Figure 4e). The above results showed that the chiral sensing performance of the proposed pure COF membrane nanochannel was much better than that of the commercial artificial AAO nanochannel.

Universality of the Developed COF Nanochannel Platform for Chiral Sensing. Three representative chiral flavor substances (*R*/*S*-propanediol, *R*/*S*-methylbutyric acid, and *R*/*S*-butanol) were selected to show the universality of the developed pure COF membrane nanochannel assay. The gating ratio and selectivity for the sensing of the chiral flavor substances are listed in Table 1. The gating ratio of the *S*-flavor enantiomers was greater than that of the *R*-flavor enantiomers for each pair of enantiomers. Meanwhile, the selectivity values for *R*/*S*-propanediol, *R*/*S*-methylbutyric acid, and *R*/*S*-butanol were 1.33, 2.52, and 2.34, respectively, suggesting that the developed pure COF nanochannel platform was generally suitable for sensing other chiral flavor enantiomers.[55] Moreover, the developed pure COF membrane nanochannel platform was successfully applied to sensing flavor substances with the enantiomer excess (ee) values of 55.2% (propanediol) and 72.4% (limonene) and the low detection limits of 36 (limonene) and 71 (propanediol) ng L^{-1} (Table 2).

Table 1. Gating Ratio and Selectivity of the Pure COF Membrane Nanochannel for Different Chiral Flavor Substances

chiral flavor substances	gating ratio	selectivity
(*S*/*R*)-(∓)-limonene	50.5/14.9	3.4
(*S*/*R*)-(±)-1,2-propanediol	10.3/7.7	1.3
(*S*/*R*)-2-methylbutyric acid	11.0/4.4	2.5
(*S*/*R*)-(±)-2-butanol	9.5/4.1	2.3

Table 2. LODs and ee Values of the Pure COF Membrane Nanochannel for Different Chiral Flavor Substances

chiral flavor substances	LODs (ng L^{-1})	ee (%)
limonene	36	72.4
propanediol	71	55.2
methylbutyric acid	48	68.2
butanol	55	62.5

CONCLUSIONS

In summary, we have developed a label-free biomimetic nanochannel sensing platform based on a pure COF membrane and chiral AuNPs selector for the sensitive and selective sensing of chiral flavor substances. The use of the pure COF membrane as a nanochannel enables quantum-confined superfluidics and surface-charge-governed ion transport within the channels for chiral sensing. The developed COF membrane nanochannel sensing platform not only allows an easy balance of the permeability and selectivity, which is difficult in traditional polymer membrane nanochannel sensors, but also exhibits better chiral performance than commercial artificial AAO nanochannel sensors. This work shows that the pure COF membrane nanosensor is promising for sensitive and selective sensing of enantiomers. Further effort should be made to develop a sensor for the differential sensing of multiple chiral flavor molecules simultaneously.

ASSOCIATED CONTENT

Supporting Information

The Supporting Information is available free of charge at https://pubs.acs.org/doi/10.1021/acssensors.3c01849.

Supplementary figures: photo, cross-sectional SEM, PXRD, FT-IR, *I*−*V* curves, ionic conductivity, and stability of the COF membrane; three-dimensional diagram of limonene, propanediol, methylbutanoic acid, and butanol; CD spectra, time-dependent hydrodynamic size, time-dependent UV−vis spectra, and effect of D/L-Cys-AuNPs; *I*−*V* curves and ionic conductivity of the AAO nanochannel; calibration curve; contact angles, zeta potential, particle size, TEM, and SEM of L-Cys-AuNPs and *R*/*S*-limonene. Supplementary tables: binding energy; intra- and interassay precisions; comparison of analytical properties; gating ratio and selectivity of D/L-Pen-AuNPs to limonene enantiomers (PDF)

AUTHOR INFORMATION

Corresponding Author

Xiu-Ping Yan − *State Key Laboratory of Food Science and Resources, International Joint Laboratory on Food Safety, Institute of Analytical Food Safety, School of Food Science and Technology, and Key Laboratory of Synthetic and Biological Colloids, Ministry of Education, Jiangnan University, Wuxi 214122, China;* orcid.org/0000-0001-9953-7681; Email: xpyan@jiangnan.edu.cn

Authors

Chen-Yan Zheng − *State Key Laboratory of Food Science and Resources, International Joint Laboratory on Food Safety, and Institute of Analytical Food Safety, School of Food Science and Technology, Jiangnan University, Wuxi 214122, China*

Hai-Long Qian − *State Key Laboratory of Food Science and Resources, International Joint Laboratory on Food Safety, and Institute of Analytical Food Safety, School of Food Science and Technology, Jiangnan University, Wuxi 214122, China;* orcid.org/0000-0001-7554-4115

Cheng Yang − *Institute of Analytical Food Safety, School of Food Science and Technology, Jiangnan University, Wuxi 214122, China*

Xu-Qin Ran − *Institute of Analytical Food Safety, School of Food Science and Technology, Jiangnan University, Wuxi 214122, China*

Complete contact information is available at: https://pubs.acs.org/10.1021/acssensors.3c01849

Notes

The authors declare no competing financial interest.

ACKNOWLEDGMENTS

The authors thank the financial support from the National Natural Science Foundation of China (no. 22176073), the Postgraduate Research & Practice Innovation Program of Jiangsu Province (no. 1022050205238490), and the Program of "Collaborative Innovation Center of Food Safety and Quality Control in Jiangsu Province".

REFERENCES

(1) Xue, Y. P.; Cao, C. H.; Zheng, Y. G. Enzymatic asymmetric synthesis of chiral amino acids. *Chem. Soc. Rev.* **2018**, *47* (4), 1516−1561.

(2) Yoo, S.; Park, Q. H. Metamaterials and chiral sensing: a review of fundamentals and applications. *Nanophotonics* **2019**, *8* (2), 249−261.

(3) Wen, Y.; He, M. Q.; Yu, Y. L.; Wang, J. H. Biomolecule-mediated chiral nanostructures: a review of chiral mechanism and application. *Adv. Colloid Interface Sci.* **2021**, *289*, No. 102376.

(4) D'Orazio, G.; Fanali, C.; Asensio-Ramos, M.; Fanali, S. Chiral separations in food analysis. *Trends Anal. Chem.* **2017**, *96*, 151−171.

(5) Tominaga, T.; Niclass, Y.; Frérot, E.; Dubourdieu, D. Stereoisomeric distribution of 3-mercaptohexan-1-ol and 3-mercaptohexyl acetate in dry and sweet white wines made from Vitis vinifera (Var. Sauvignon Blanc and Semillon). *J. Agric. Food Chem.* **2006**, *54* (19), 7251−7255.

(6) Ebeler, S. E., Enantiomeric Analysis as a Tool for Authentication of Foods and Beverages. In *Authentication of Food and Wine*, Chapter 3, ACS Symposium Series, American Chemical Society, WA, 2006, *952* pp 39−49 DOI: 10.1021/bk-2007-0952.ch003.

(7) Rocco, A.; Aturki, Z.; Fanali, S. Chiral separations in food analysis. *Trends Anal. Chem.* **2013**, *52*, 206−225.

(8) Engel, K. H. Chirality: An important phenomenon regarding biosynthesis, perception, and authenticity of flavor compounds. *J. Agric. Food Chem.* **2020**, *68* (38), 10265−10274.

(9) Ribeiro, C.; Gonçalves, R.; Tiritan, M. E. Separation of enantiomers using gas chromatography: application in forensic toxicology, food and environmental analysis. *Crit. Rev. Anal. Chem.* **2021**, *51* (8), 787−811.

(10) Begnaud, F.; Starkenmann, C.; Van de Waal, M.; Chaintreau, A. Chiral multidimensional gas chromatography (MDGC) and chiral GC-olfactometry with a double-cool-strand interface: application to malodors. *Chem. Biodivers.* **2006**, *3* (2), 150−160.

(11) Alajmi, M. F.; Hussain, A.; Suhail, M.; Mukhtar, S. D.; Sahoo, D. R.; Asnin, L.; Ali, I. Chiral HPLC separation and modeling of four stereomers of DL-Leucine-DL-Tryptophan dipeptide on amylose chiral column. *Chirality* **2016**, *28* (9), 642−648.

(12) Mei, X.; Wolf, C. Enantioselective sensing of chiral carboxylic acids. *J. Am. Chem. Soc.* **2004**, *126*, 14736−14737.

(13) Zhang, M.; Ye, B. C. Colorimetric chiral recognition of enantiomers using the nucleotide-capped silver nanoparticles. *Anal. Chem.* **2011**, *83* (5), 1504−1509.

(14) Ding, S.; Cao, S.; Zhu, A.; Shi, G. Wettability switching of electrode for signal amplification: conversion of conformational change of stimuli-responsive polymer into enhanced electrochemical chiral analysis. *Anal. Chem.* **2016**, *88* (24), 12219−12226.

(15) Yu, Y.; Tao, Y.; Yang, B.; Wu, D.; Qin, Y.; Kong, Y. Smart chiral sensing platform with alterable enantioselectivity. *Anal. Chem.* **2017**, *89* (23), 12930−12937.

(16) Yang, J.; Yu, Y.; Wu, D.; Tao, Y.; Deng, L.; Kong, Y. Coinduction of a chiral microenvironment in polypyrrole by overoxidation and camphorsulfonic acid for electrochemical chirality sensing. *Anal. Chem.* **2018**, *90* (15), 9551−9558.

(17) Bian, G.; Yang, S.; Huang, H.; Zong, H.; Song, L. A bisthiourea-based 1 H NMR chiral sensor for chiral discrimination of a variety of chiral compounds. *Sens. Actuators B Chem.* **2016**, *231*, 129−134.

(18) Zor, E.; Bingol, H.; Ersoz, M. Chiral sensors. *Trends Anal. Chem.* **2019**, *121*, No. 115662.

(19) Bernardo-Bermejo, S.; Sánchez-López, E.; Castro-Puyana, M.; Marina, M. L. Chiral capillary electrophoresis. *Trends Anal. Chem.* **2020**, *124*, No. 115807.

(20) Liu, X.; Lu, J.; Chen, J.; Zhang, M.; Chen, Y.; Xing, F.; Feng, L. Chiral self-assembly of porphyrins induced by chiral carbon dots. *Front. Chem.* **2020**, *8*, 670.

(21) Zhang, H.; Tian, Y.; Jiang, L. From symmetric to asymmetric design of bio-inspired smart single nanochannels. *ChemComm.* **2013**, *49* (86), 10048−10063.

(22) Hou, X. Smart gating multi-scale pore/channel-based membranes. *Adv. Mater.* **2016**, *28* (33), 7049−7064.

(23) Xiao, K.; Wen, L.; Jiang, L. Biomimetic solid-state nanochannels: from fundamental research to practical applications. *Small* **2016**, *12* (21), 2810−2831.

(24) Li, R.; Fan, X.; Liu, Z.; Zhai, J. Zhai, Smart bioinspired nanochannels and their applications in energy-conversion systems. *Adv. Mater.* **2017**, *29* (45), 1702983.

(25) Zhang, S.; Li, K. B.; Pan, Y.; Han, D. M. Ultrasensitive detection of ochratoxin A based on biomimetic nanochannel and catalytic hairpin assembly signal amplification. *Talanta* **2020**, *220*, No. 121420.

(26) Cheng, J.; Jiang, F.; Zhang, S. A nanofluidic device for ultrasensitive and label-free detection of tetracycline in association with gamma-cyclodextrin and GO. *Anal. Methods* **2021**, *13* (15), 1832−1838.

(27) Kan, X.; Wu, C.; Wen, L.; Jiang, L. Biomimetic nanochannels: from fabrication principles to theoretical insights. *Small Methods* **2022**, *6* (4), No. e2101255.

(28) Xiao, K.; Wan, C.; Jiang, L.; Chen, X.; Antonietti, M. Bioinspired ionic sensory systems: the successor of electronics. *Adv. Mater.* **2020**, *32* (31), No. e2000218.

(29) Zhu, Z.; Wang, D.; Tian, Y.; Jiang, L. Ion/molecule transportation in nanopores and nanochannels: from critical principles to diverse functions. *J. Am. Chem. Soc.* **2019**, *141* (22), 8658−8669.

(30) Xu, Y.; Sui, X.; Guan, S.; Zhai, J.; Gao, L. Olfactory sensory neuron-mimetic CO_2 activated nanofluidic diode with fast response rate. *Adv. Mater.* **2015**, *27* (11), 1851−1855.

(31) Bayley, H.; Cremer, P. S. Stochastic sensors inspired by biology. *Nature* **2001**, *413* (6852), 226−230.

(32) Cooper, J. A.; Borsley, S.; Lusby, P. J.; Cockroft, S. L. Discrimination of supramolecular chirality using a protein nanopore. *Chem. Sci.* **2017**, *8* (7), 5005−5009.

(33) Rauf, S.; Zhang, L.; Ali, A.; Liu, Y.; Li, J. Label-free nanopore biosensor for rapid and highly sensitive cocaine detection in complex biological fluids. *ACS Sens.* **2017**, *2* (2), 227−234.

(34) Liu, Q.; Xiao, K.; Wen, L.; Lu, H.; Liu, Y.; Kong, X. Y.; Xie, G.; Zhang, Z.; Bo, Z.; Jiang, L. Engineered ionic gates for ion conduction based on sodium and potassium activated nanochannels. *J. Am. Chem. Soc.* **2015**, *137* (37), 11976−11983.

(35) Zhang, F.; Sun, Y.; Tian, D.; Li, H. Chiral selective transport of proteins by cysteine-enantiomer-modified nanopores. *Angew. Chem., Int. Ed.* **2017**, *56* (25), 7186−7190.

(36) Sun, Y.; Zhang, F.; Quan, J.; Zhu, F.; Hong, W.; Ma, J.; Pang, H.; Sun, Y.; Tian, D.; Li, H. A biomimetic chiral-driven ionic gate constructed by pillar[6]arene-based host-guest systems. *Nat. Commun.* **2018**, *9* (1), 2617.

(37) Zhang, X.; Zhang, F.; Zhu, F.; Zhang, X.; Tian, D.; Johnson, R. P.; Li, H. Bioinspired gamma-cyclodextrin pseudorotaxane assembly nanochannel for selective amino acid transport. *ACS Appl. Bio. Mater.* **2019**, *2* (8), 3607−3612.

(38) Zhang, S.; Cheng, M.; Dhinakaran, M. K.; Sun, Y.; Li, H. Enantioselective antiport in asymmetric nanochannels. *ACS Nano* **2021**, *15* (8), 13148−13154.

(39) Yan, F.; Yao, L.; Yang, Q.; Chen, K.; Su, B. Ionic current rectification by laminated bipolar silica isoporous membrane. *Anal. Chem.* **2019**, *91* (2), 1227−1231.

(40) Han, C.; Hou, X.; Zhang, H.; Guo, W.; Li, H.; Jiang, L. Enantioselective recognition in biomimetic single artificial nanochannels. *J. Am. Chem. Soc.* **2011**, *133* (20), 7644−7647.

(41) Sun, Z.; Zhang, F.; Zhang, X.; Tian, D.; Jiang, L.; Li, H. Chiral recognition of Arg based on label-free PET nanochannel. *ChemComm.* **2015**, *51* (23), 4823−4826.

(42) Meng, D.; Hao, C.; Cai, J.; Ma, W.; Chen, C.; Xu, C.; Xu, L.; Kuang, H. Tailored chiral copper selenide nanochannels for ultrasensitive enantioselective recognition and detection. *Angew. Chem., Int. Ed.* **2021**, *60* (47), 24997−25004.

(43) Ding, S. Y.; Wang, W. Covalent organic frameworks (COFs): from design to applications. *Chem. Soc. Rev.* **2013**, *42* (2), 548−568.

(44) Guo, J.; Xu, Y.; Jin, S.; Chen, L.; Kaji, T.; Honsho, Y.; Addicoat, M. A.; Kim, J.; Saeki, A.; Ihee, H.; Seki, S.; Irle, S.; Hiramoto, M.;

https://doi.org/10.1021/acssensors.3c01849
ACS Sens. 2023, 8, 4747−4755

Gao, J.; Jiang, D. Conjugated organic framework with three-dimensionally ordered stable structure and delocalized pi clouds. *Nat. Commun.* **2013**, *4*, 2736.
(45) Segura, J. L.; Mancheno, M. J.; Zamora, F. Covalent organic frameworks based on Schiff-base chemistry: synthesis, properties and potential applications. *Chem. Soc. Rev.* **2016**, *45* (20), 5635−5671.
(46) Li, H.-Z.; Yang, C.; Qian, H.-L.; Yan, X.-P. Room-temperature synthesis of ionic covalent organic frameworks for efficient removal of diclofenac sodium from aqueous solution. *Sep. Purif. Technol.* **2023**, *306*, No. 122704, DOI: 10.1016/j.seppur.2022.122704.
(47) Yuan, C.; Wu, X.; Gao, R.; Han, X.; Liu, Y.; Long, Y.; Cui, Y. Nanochannels of covalent organic frameworks for chiral selective transmembrane transport of amino acids. *J. Am. Chem. Soc.* **2019**, *141* (51), 20187−20197.
(48) Ran, X. Q.; Qian, H. L.; Yan, X. P. Integrating ordered two-dimensional covalent organic frameworks to solid-state nanofluidic channels for ultrafast and sensitive detection of mercury. *Anal. Chem.* **2022**, *94* (23), 8533−8538.
(49) Hou, S.; Ji, W.; Chen, J.; Teng, Y.; Wen, L.; Jiang, L. Free-standing covalent organic framework membrane for high-efficiency salinity gradient energy conversion. *Angew. Chem., Int. Ed.* **2021**, *60* (18), 9925−9930.
(50) Wang, S.; Yang, L.; Xu, K.; Chen, H.; Huang, N. De novo fabrication of large-area and self-standing covalent organic framework films for efficient separation. *ACS Appl. Mater. Interfaces* **2021**, *13* (37), 44806−44813.
(51) Liu, J.; Han, G.; Zhao, D.; Lu, K.; Gao, J.; Chung, T. S. Self-standing and flexible covalent organic framework (COF) membranes for molecular separation. *Sci. Adv.* **2020**, *6*, No. eabb1110.
(52) Li, Y.; Wu, Q.; Guo, X.; Zhang, M.; Chen, B.; Wei, G.; Li, X.; Li, X.; Li, S.; Ma, L. Laminated self-standing covalent organic framework membrane with uniformly distributed subnanopores for ionic and molecular sieving. *Nat. Commun.* **2020**, *11* (1), 599.
(53) Zhang, S.; Zhou, J.; Li, H. Chiral covalent organic framework packed nanochannel membrane for enantioseparation. *Angew. Chem., Int. Ed.* **2022**, *61* (27), No. e202204012.
(54) Wen, L.; Zhang, X.; Tian, Y.; Jiang, L. Quantum-confined superfluid: From nature to artificial. *Sci. China Mater.* **2018**, *61* (8), 1027−1032.
(55) Wu, M. Y.; Mo, R. J.; Ding, X. L.; Huang, L. Q.; Li, Z. Q.; Xia, X. H. Homochiral zeolitic imidazolate framework with defined chiral microenvironment for electrochemical enantioselective recognition. *Small* **2023**, *19*, No. e2301460.
(56) Fair, J. C.; Osterle, J. F. Reverse electrodialysis in charged capillary membranes. *J. Chem. Phys.* **1971**, *54* (8), 3307−3316.
(57) Boussouar, I.; Chen, Q.; Chen, X.; Zhang, Y.; Zhang, F.; Tian, D.; White, H. S.; Li, H. Single nanochannel platform for detecting chiral drugs. *Anal. Chem.* **2017**, *89* (2), 1110−1116.
(58) Huang, L.; Lin, Q.; Li, Y.; Zheng, G.; Chen, Y. Study of the enantioselectivity and recognition mechanism of sulfhydryl-compound-functionalized gold nanochannel membranes. *Anal. Bioanal. Chem.* **2019**, *411* (2), 471−478.
(59) Basu, S.; Paul, A.; Chattopadhyay, A. Zinc-coordinated hierarchical organization of ligand-stabilized gold nanoclusters for chiral recognition and separation. *Chemistry* **2017**, *23* (38), 9137−9143.
(60) Ran, X. Q.; Qian, H. L.; Yan, X. P. Aptamer self-assembly-functionalized nanochannels for sensitive and precise detection of chloramphenicol. *Anal. Chem.* **2021**, *93* (42), 14287−14292.

https://doi.org/10.1021/acssensors.3c01849
ACS Sens. 2023, 8, 4747−4755